The Astronomical Journal, 159:216 (15pp), 2020 May https://doi.org/10.3847/1538-3881/ab7db5

Low-mass Group Environments Have No Substantial Impact on the Circumgalactic Medium Metallicity

Stephanie K. Pointon[1,2], Glenn G. Kacprzak[1,2], Nikole M. Nielsen[1,2], Michael T. Murphy[1], Sowgat Muzahid[3], Christopher W. Churchill[4], and Jane C. Charlton[5]
[1] Centre for Astrophysics and Supercomputing, Swinburne University of Technology, Hawthorn, VIC 3122, Australia; spointon@swin.edu.au
[2] ARC Centre of Excellence for All Sky Astrophysics in 3 Dimensions (ASTRO 3D), Australia
[3] Leiden Observatory, University of Leiden, P.O. Box 9513, NL-2300 RA Leiden, The Netherlands
[4] Department of Astronomy, New Mexico State University, Las Cruces, NM 88003, USA
[5] Department of Astronomy and Astrophysics, The Pennsylvania State University, State College, PA 16801, USA
Received 2019 August 12; revised 2020 March 3; accepted 2020 March 5; published 2020 April 16

Abstract

We explore how environment affects the metallicity of the circumgalactic medium (CGM) using 13 low-mass galaxy groups (two to five galaxies) at $\langle z_{\rm abs}\rangle = 0.25$ identified near background quasars. Using quasar spectra from the *Hubble Space Telescope*/COS and from Keck/HIRES or the Very Large Telescope/UVES, we measure column densities of or determine limits on CGM absorption lines. We use a Markov Chain Monte Carlo approach with Cloudy to estimate metallicities of cool ($T \sim 10^4$ K) CGM gas within groups and compare them to CGM metallicities of 47 isolated galaxies. Both group and isolated CGM metallicities span a wide range ($-2 <$ [Si/H] < 0), where the mean group (-0.54 ± 0.22) and isolated (-0.77 ± 0.14) CGM metallicities are similar. Group and isolated environments have similar distributions of H I column densities as a function of impact parameter. However, contrary to isolated galaxies, we do not find an anticorrelation between H I column density and the nearest group galaxy impact parameter. We additionally divided the groups by member luminosity ratios (i.e., galaxy–galaxy and galaxy–dwarf groups). While there was no significant difference in their mean metallicities, a modest increase in sample size should allow one to statistically identify a higher CGM metallicity in galaxy–dwarf groups compared to galaxy–galaxy groups. We conclude that either environmental effects have not played an important role in the metallicity of the CGM at this stage and expect that this may only occur when galaxies are strongly interacting or merging or that some isolated galaxies have higher CGM metallicities due to past interactions. Thus, environment does not seem to be the cause of the CGM metallicity bimodality.

Unified Astronomy Thesaurus concepts: Circumgalactic medium (1879); Quasar absorption line spectroscopy (1317); Metallicity (1031); Galaxy environments (2029)

Supporting material: figure sets, machine-readable table

1. Introduction

The gas surrounding galaxies outside their disks/interstellar medium (ISM) and residing within their virial radii is known as the circumgalactic medium (CGM; Tumlinson et al. 2017). Our understanding of the CGM has mainly been derived from studies of isolated galaxies revealing that within $1\,R_{\rm vir}$, the CGM contains a mass comparable to the ISM and is comprised of accreting, outflowing, and recycling gas (e.g., Kacprzak et al. 2008, 2011, 2016; Chen et al. 2010a; Thom et al. 2011; Tumlinson et al. 2011; Rudie et al. 2012; Nielsen et al. 2013a, 2013b; Werk et al. 2013; Peeples et al. 2014).

It is expected that the CGM in group environments would be affected by galaxy–galaxy interactions and hence be more complex. The effects of galaxy–galaxy interactions are clearly visible as tidal streams in H I emission around the M81/M82 galaxy group (Yun et al. 1994; Chynoweth et al. 2008; de Blok et al. 2018). Further observations of H I gas in the CGM have found evidence for interactions in the form of tidal streams, warped disks, and high-velocity clouds (e.g., Puche et al. 1992; Swaters et al. 1997; Rand 2000; Fraternali et al. 2002; Chynoweth et al. 2008; Sancisi et al. 2008; Mihos et al. 2012; Wolfe et al. 2013). Additionally, absorption studies of group environment CGM gas have detected the presence of tidal streams or intragroup gas (Whiting et al. 2006; Kacprzak et al. 2010; Nestor et al. 2011; Gauthier 2013; Bielby et al. 2017; Péroux et al. 2017; Pointon et al. 2017; Nielsen et al. 2018; Chen et al. 2019). The tidal streams and increased star formation rates that occur during mergers have been suggested to increase the halo gas mass and cross section (York et al. 1986; Rubin et al. 2010). Furthermore, FIRE simulations have demonstrated that intergalactic transfer is the dominant mode of gas accretion for $z < 1$ (Anglés-Alcázar et al. 2017). These combined results suggest that group environments cause the CGM to be disrupted, similar to the stellar components of interacting galaxies. Given the large inferred size of the CGM ($\sim$200 kpc for L_* galaxies at redshifts $z < 1.0$; Tumlinson et al. 2011; Werk et al. 2014), it is possible that the CGM will be influenced by a merger before the visible components of the host galaxy (Nielsen et al. 2018).

Using Mg II as a tracer of cool gas in cluster environments, Lopez et al. (2008) detected an overabundance of strong Mg II absorbers near clusters compared to field galaxies. A similar enhancement of weak Mg II absorbers beyond the cluster center was not observed, consistent with expectations that these absorbers should be destroyed by the hot cluster environment. The distributions of the weak and strong Mg II absorbers within the cluster is then evidence for a truncated cold gas halo, consistent with simulations (Padilla et al. 2009; Andrews et al. 2013).

Chen et al. (2010a) investigated group environments using Mg II as a tracer of cool gas. In seven out of eight of the group

environments identified, Mg II was detected. While the group environment Mg II absorption appeared to span the same equivalent width versus impact parameter range as isolated galaxies, the authors did not detect a significant anticorrelation. This is contrary to the strong and well-known anticorrelation for isolated galaxies (e.g., Lanzetta & Bowen 1990; Steidel et al. 1994; Chen & Tinker 2008; Kacprzak et al. 2008, 2012; Chen et al. 2010b; Bordoloi et al. 2011; Nielsen et al. 2013a). Indeed, Nielsen et al. (2013a) found the anticorrelation between Mg II equivalent width and impact parameter for isolated galaxies to be highly significant (7.9σ).

Further studies have found that the radial distribution of Mg II is flatter in group environments compared to isolated galaxies (e.g., Bordoloi et al. 2011; Nielsen et al. 2018). Bordoloi et al. (2011) found that the average Mg II equivalent widths decreased beyond 140 kpc in group environments, whereas they began to decrease beyond 70 kpc for isolated galaxies. They further found that the radial distribution for the group environments CGM is consistent with a superposition of individual overlapping halos. Thus, the authors suggested that the group environment CGM is not strongly influenced by tidal stripping or outflows driven by increased star formation. However, using the kinematic structure of Mg II absorbers in group environments, Nielsen et al. (2018) found that a superposition model can reproduce the equivalent widths required but overpredicts absorption at high velocities due to the large velocity separations between the galaxies in the group. Instead, the authors suggest that the cool gas in group environments forms an intragroup medium, created by intergalactic transfer or tidal stripping.

Major mergers are able to disrupt the structure of involved galaxies more than minor mergers. Thus, it is possible that the type of merger/interaction affects the CGM gas differently. Nielsen et al. (2018) found that galaxy–galaxy groups (where the two brightest galaxies have similar luminosities, $L_1/L_2 < 3.5$) may have larger equivalent widths (1.7σ) and absorber velocity dispersions (2.5σ) than galaxy–dwarf groups ($L_1/L_2 \geqslant 3.5$), while the covering fractions for the two samples are consistent within the uncertainties. They suggest that tidal stripping of CGM gas and increased star formation might be more likely to occur in galaxy–galaxy groups.

The cool gas in the CGM, traced by Mg II, is likely to be constrained to high-density structures surrounded by highly ionized gas traced by C IV and O VI. This highly ionized gas has also been investigated in group environments (e.g., Stocke et al. 2013; Burchett et al. 2016; Pointon et al. 2017; Ng et al. 2019). Burchett et al. (2016) found that as the number of galaxies in a group increases, the C IV equivalent width decreases, with no C IV detected in groups with more than seven galaxies. Similarly, O VI has lower velocity spreads and column densities in group environments compared to isolated environments (Stocke et al. 2013; Pointon et al. 2017; Ng et al. 2019). These results are consistent with the picture that the virial temperature, which scales with halo mass, leads to oxygen and carbon ionizing to higher states than O VI and C IV, respectively (Oppenheimer et al. 2016; Bielby et al. 2019; Ng et al. 2019; Zahedy et al. 2019).

All of this evidence suggests that it is possible for CGM metallicities to also be impacted by environment. Simulations by Hani et al. (2018) investigated the changes in CGM metallicity during a major merger. The authors found that, compared to the premerger state, the metallicity of the gas increased during the merger by 0.2–0.3 dex. The increase was driven by outflows from the increased star formation caused by the merger, rather than tidal stripping, and this metallicity level was maintained for several billions of years postmerger. This evidence that major mergers are capable of changing the CGM metallicity provides incentive for studying the metallicity of group environments premerger as a baseline.

Preliminary results from Lehner (2017) compare high- and low-metallicity absorbers from both isolated and group environments. They found that for partial Lyman limit systems (pLLs; $16.2\ \mathrm{cm^{-2}} < \log N_{\mathrm{H\,I}} < 17.2\ \mathrm{cm^{-2}}$) and Lyman limit systems (LLS; $17.2\ \mathrm{cm^{-2}} < \log N_{\mathrm{H\,I}} < 19.0\ \mathrm{cm^{-2}}$), the high-metallicity systems are more likely to be associated with group environments, while the low-metallicity systems are associated with isolated environments. While the authors cautioned that this result is preliminary and refrained from making any interpretations, it may suggest that interactions in groups of galaxies may be causing increased metallicity. This result is somewhat challenged by Pointon et al. (2019), who studied the metallicity of the CGM in isolated environments. They found that the CGM metallicities of isolated galaxies span the full range detected by Lehner (2017), even when the sample is restricted to the same H I column density range. This suggests that high-metallicity systems are not only found in group environments.

Following from Lehner (2017), we investigate the effect of environment on the metallicity of the CGM by comparing the isolated galaxy sample from Pointon et al. (2019) to group environments. We investigate the metallicity of 13 group environments using the combination of UV spectra from the Hubble Space Telescope (HST)/Cosmic Origins Spectrograph (COS) and Far-Ultraviolet Spectroscopic Explorer (FUSE), as well as optical spectra from the Keck/High Resolution Echelle Spectrometer (HIRES) and Very Large Telescope (VLT)/UVES.

This paper is organized as follows. In Section 2 we describe our sample of group galaxy–absorber pairs. We also describe how we obtain the metallicity of the CGM. We present the results comparing the group environment CGM metallicity with the same properties for isolated galaxies and investigate any trends with H I column density, impact parameter, and luminosity in Section 4; we discuss the implications in Section 5. In Section 6 we summarize our results and provide concluding remarks. We use a standard ΛCDM cosmology with $H_o = 70\ \mathrm{km\ s^{-1}\ Mpc^{-1}}$, $\Omega_M = 0.3$, and $\Omega_\Lambda = 0.7$.

2. Observations

In order to study the CGM of the group environments, we use the "Multiphase Galaxy Halos" Survey, which is comprised of UV HST/COS spectra from our program (PID 13398; Kacprzak et al. 2015, 2019; Muzahid et al. 2015, 2016; Nielsen et al. 2017; Pointon et al. 2017, 2019; Ng et al. 2019), as well as data taken from the literature (Chen et al. 2001b; Chen & Mulchaey 2009; Meiring et al. 2011; Werk et al. 2012; Johnson et al. 2013). A group environment is defined as having the nearest of two or more galaxies within 18–150 kpc of the quasar sight line in order to replicate the impact parameter distribution of the isolated sample. The galaxies in the group must have line-of-sight velocity separations of less than 1000 km s^{-1} and a maximum impact parameter of 500 kpc. We investigate 13 group environments from the literature for which we have UV spectra (Lanzetta et al. 1995; Chen et al.

Table 1
Quasar Observations

J-Name (1)	z_{qso} (2)	R.A. (J2000) (3)	Decl. (J2000) (4)	UV Inst. (5)	COS Gratings (6)	COS PID(s) (7)	Optical Spectrograph (8)	Optical PID(s) (9)
J0125	1.074	01:25:28.84	−00:05:55.93	COS	G160M	13398	UVES	075.A-0841(A)
J0228	0.493	02:28:15.17	−40:57:14.29	COS	G130M, G160M	11541	⋯	⋯
J0351	0.616	03:51:28.54	−14:29:08.71	COS	G130M, G160M	13398	UVES	076.A-0860(A)
J0407	0.572	04:07:48.43	−12:11:36.66	COS, FUSE	G130M, G160M	11541	HIRES	G01H, U68H
J0853	0.514	08:53:34.25	+43:49:02.33	COS	G130M, G160M	13398	⋯	⋯
J0910	0.463	09:10:29.75	+10:14:13.61	COS	G130M, G160M	11598	⋯	⋯
J0925	0.472	09:25:54.71	+40:04:14.17	COS	G130M, G160M	11598	HIRES	U059Hb
J0928	0.296	09:28:37.98	+60:25:21.02	COS	G130M, G160M	11598	HIRES	U066Hb
J1009	0.456	10:09:02.06	+07:13:43.87	COS	G130M, G160M	11598	HIRES	U066Hb
J1119	0.176	11:19:08.67	+21:19:18.01	COS, FUSE	G130M, G160M	12038	HIRES	U152Hb
J1139	0.556	11:39:10.70	−13:50:43.63	COS	G130M	12275	⋯	⋯

2001b; Chen & Mulchaey 2009; Prochaska et al. 2011; Werk et al. 2012; Johnson et al. 2015; Muzahid et al. 2015; Nielsen et al. 2018). The groups have associated H I absorption with a redshift range of $0.06 < z_{abs} < 0.38$ ($\langle z_{abs} \rangle = 0.25$). The group environments have a wide range of luminosity ratios between the brightest (L_1) and second-brightest (L_2) galaxies ($1.1 < L_1/L_2 < 27.7$; median $L_1/L_2 = 2.7$), indicating that we are investigating groups with a variety of mass ratios. Typical group environments in this study have two members, although J0407, $z_{abs} = 0.0914$, has five galaxies, with a mean of 2.2 galaxies per group. We note that group environments range from galaxy–dwarf pairs to clusters of galaxies. Therefore, our study probes the low-mass end of group environments.

All quasars in the sample have COS UV spectra, while two also have reduced UV spectra from the FUSE telescope, provided by B. Wakker (2016, private communication). Eight quasars have optical spectra from Keck/HIRES or VLT/UVES. The details of the quasar spectra are shown in Table 1.

2.1. UV Quasar Spectra

The COS quasar spectra used in our survey have a median resolving power of $R \approx 20{,}000$, while the FUSE quasar spectra have a resolving power of $R \approx 30{,}000$. The instruments, gratings, and PID(s) for both COS and FUSE quasar spectra are in Table 1. The range of ions covered by the UV spectra includes the H I Lyman series, C II, C III, C IV, N II, N III, N V, O I, O VI, Si II, Si III, and Si IV. The reduction process for the HST/COS spectra is described in detail in Kacprzak et al. (2015). The raw data were reduced using the CALCOS pipeline software and then flux-calibrated. Individual grating integrations were coadded and rebinned by 3 pixels to improve the signal-to-noise ratio (Danforth et al. 2010).[6] The COS and FUSE UV spectra were then continuum-normalized by fitting low-order polynomials to the spectra while excluding absorption and emission lines from the fitting region.

2.2. Optical Quasar Spectra

The UV spectra were complemented by additional optical spectra, which cover ionic transitions including Mg I, Mg II, Fe II, Mn II, and Ca II for redshifts of $z > 0.2$. Eight quasars have optical spectra from Keck/HIRES and VLT/UVES with a resolving power of $R \approx 40{,}000$. The spectrograph and PID(s) for the optical spectra are in Table 1. The Maunakea Echelle Extraction package or IRAF were used to reduce the HIRES data. The UVES spectra were reduced using the European Southern Observatory pipeline (Dekker et al. 2000) and the UVES Post-Pipeline Echelle Reduction (UVES POPLER) code (Murphy 2016; Murphy et al. 2019).

2.3. Optical Galaxy Spectra

Optical spectra of the galaxies in three group environment quasar fields were obtained using the Keck Echelle Spectrograph and Imager (Sheinis et al. 2002), since the wavelength range (4000–10000 Å) provides coverage of emission lines including Hα. The reduction method is described in Nielsen et al. (2018), Kacprzak et al. (2019), and Pointon et al. (2019). However, we summarize the process here. The data, taken through slits of 20″ by 1″, were binned by two, resulting in a spatial pixel size of 0.″27–0.″34 and a spectral resolution of 22 km s^{-1}. The reduction process was completed using IRAF, after which heliocentric and vacuum corrections were applied to the data. Galaxy redshifts are shown in column (2) of Table 2. The redshifts for the remaining galaxies were obtained from the literature, indicated in column (3) of Table 2.

2.4. Isolated Galaxy Sample

We use the metallicity study of 47 isolated environments by Pointon et al. (2019) with a redshift range of $0.06 < z < 0.66$ ($\langle z \rangle = 0.27$) to compare to the group environments. An isolated galaxy is defined as having no neighboring galaxies within a spatial separation of 150 kpc and line-of-sight velocity separation of 1000 km s^{-1}. Where the spatial or kinematic criteria were not met, the system was classified as a group environment. The impact parameters are in the range 18 kpc $< D <$ 203 kpc. The isolated galaxies are roughly L_* galaxies, with a halo mass range of $10.8 < \log M_h/M_\odot < 12.5$ ($\langle \log M_h/M_\odot \rangle = 11.8$). The absorption systems span H I column densities in the range $13.8 < \log N_{\rm H\,I} < 19.9$. Using the same methods we use here, Pointon et al. (2019) estimated CGM metallicities in the range $-2.6 <$ [Si/H] < 0.8 with an average of $\langle$[Si/H]$\rangle = -1.3$.

2.5. Sample Comparison

The sample investigated here is a collation of quasar fields that have been previously spectroscopically surveyed (see Table 2 and Pointon et al. 2019). Consequently, each survey

[6] http://casa.colorado.edu/~danforth/science/cos/costools.html

Table 2
Galaxy Properties

J-Name	$z_{\rm gal}$	Ref.[a]	$\Delta\alpha$ (J2000)	$\Delta\delta$ (J2000)	θ (deg)	D (kpc)	M_B	L_B/L_B^*	$v_{G1}-v_{GX}$[b] (km s^{-1})
(1)	(2)	(3)	(4)	(5)	(6)	(7)	(8)	(9)	(10)
J0125	0.3787	(1)	−8.8	−12.3	15.07	78	−20.21	0.52	⋯
	0.3792	(2)	−27.7	−36.5	45.80	238	−20.21	0.57	108
J0228	0.2065	(3)	−9.1	−8.4	10.87	34	−19.42	0.32	⋯
	0.2078	(3)	−24.9	−25.9	32.04	109	−18.32	0.15	323
J0228	0.2678	(3)	16.9	−13.0	18.21	63	−19.43	0.29	⋯
	0.2690	(3)	8.5	−36.7	37.26	154	−16.78	0.02	284
	0.2680	(3)	36.2	−29.2	39.98	164	−18.01	0.08	47
J0351	0.324180	(4)	13.0	−23.5	26.72	126	−20.15	0.52	⋯
	0.324651	(4)	−29.9	18.5	34.33	162	−20.95	1.09	107
	0.3273	(2)	−59.0	19.5	60.31	288	−20.27	0.58	706
J0407	0.0923	(5)	13.6	−39.9	42.08	72	−15.45	0.01	⋯
	0.0908	(5)	−61.9	13.6	62.01	105	−15.88	0.01	−412
	0.0914	(5)	−78.9	−10.6	77.89	133	−15.84	0.01	−247
	0.0917	(5)	−123.5	−127.3	175.44	300	−15.12	0.01	−165
	0.0908	(5)	62.5	−252.3	259.64	439	−17.29	0.05	−412
J0407	0.16699	(4)	−1.1	34.8	34.81	99	−18.04	0.09	⋯
	0.16699	(4)	41.3	−1.8	40.36	115	−21.65	2.49	0
J0853	0.0903	(6)	14.1	−34.0	35.45	79	−18.75	0.19	⋯
	0.0915	(3)	−1.8	40.8	40.81	53	−17.28	0.05	330
J0910	0.2647	(7)	8.3	11.4	13.99	54	−19.70	0.37	⋯
	0.2641	(7)	−30.8	−16.4	34.42	132	−21.00	1.23	−142
J0925	0.2467	(7)	−7.2	−24.1	24.69	96	−20.52	0.80	⋯
	0.2475	(7)	−8.0	−20.8	21.64	84	−21.25	1.57	192
J0928	0.1540	(7)	67.2	−12.3	35.38	95	−20.14	0.63	⋯
	0.1542	(7)	30.2	−12.1	19.19	51	−19.84	0.48	52
	0.1537	(7)	−3.5	−14.7	14.82	40	−18.76	0.18	−78
J1009	0.35587	(4)	1.7	−9.3	9.41	47	−19.98	0.43	⋯
	0.35585	(4)	3.2	0.0	3.13	16	−17.87	0.06	−4
J1119	0.0600	(8)	−48.1	−104.9	117.01	136	−17.75	0.08	⋯
	0.0594	(8)	−83.1	−174.6	190.99	219	−16.56	0.03	−170
J1133	0.2367	(7)	4.5	−1.7	4.79	18	−21.24	1.58	⋯
	0.2364	(7)	−4.1	−9.6	10.39	39	−20.54	0.83	−73

Notes.
[a] Galaxy identification references: (1) Muzahid et al. (2015), (2) Chen et al. (2001b), (3) Chen & Mulchaey (2009), (4) Nielsen et al. (2018), (5) Johnson et al. (2015), (6) Lanzetta et al. (1995), (7) Werk et al. (2012), and (8) Prochaska et al. (2011).
[b] Line-of-sight velocity separations between the first galaxy in the group ($G1$) and each of the other group galaxy members (GX).

has different levels of completeness but typically has a luminosity sensitivity of $0.1L_*$. Fields drawn from the COS Halos survey have been probed out to a distance of 150 kpc (see Tumlinson et al. 2013; Werk et al. 2013), while other fields have been investigated out to at least 350 kpc (see Pointon et al. 2017; Nielsen et al. 2018; Kacprzak et al. 2019; Ng et al. 2019, for further details). It is possible that isolated galaxies identified in the COS Halos survey may be a member of a group that extends beyond the survey regions. To investigate this, we repeated all statistical tests with the COS Halos galaxies removed from the isolated sample. We do not find any difference in the results with the COS Halos fields removed and hence include all galaxies in our full isolated sample (Tables 3 and 6).

The isolated and group environment samples both probe a similar range of impact parameters and luminosities, as shown in Figures 1(a) and (b). The isolated galaxies are orange, the nearest group galaxy members are solid purple, and the remaining group galaxy members are hatched purple. We test the null hypothesis that the group galaxies are drawn from the same population as the isolated sample with an Anderson–Darling test and find that there is no significant difference between the impact parameter (0.4σ) and luminosity (1.8σ) distributions. The details of this test and additional Anderson–Darling tests are shown in Table 3.

Furthermore, we show the redshift distribution of isolated and group environment absorbers in Figure 1(c). Isolated galaxy–absorber pairs are shown in orange, while group environment absorbers are shown in purple. Although the

Table 3
Anderson–Darling Test Results

Variable	Anderson–Darling Test Statistic	p-value	Confidence Level	σ
Comparison of the Isolated Sample without COS Halos Galaxies with the Group Sample (see Section 2.5)				
Metallicity ([Si/H])	2.72	0.03	96.80	2.14
Average impact parameter (D)	0.15	0.98	2.15	0.03
Most luminous galaxy impact parameter (D)	0.19	0.93	6.60	0.08
Nearest galaxy impact parameter (D)	3.10	0.04	96.05	2.06
All galaxies impact parameter (D)	0.16	0.96	3.85	0.05
All galaxies luminosity (L_B/L_B^*)	2.56	0.06	93.60	1.85
All absorbers redshift (z)	1.10	0.29	70.95	1.06
Comparison of the Full Isolated Sample with the Group Sample				
Metallicity ([Si/H])	3.17	0.02	98.45	2.42
Average impact parameter (D)	0.41	0.70	30.40	0.39
Most luminous galaxy impact parameter (D)	0.28	0.88	11.70	0.15
Nearest galaxy impact parameter (D)	2.16	0.09	90.70	1.68
All galaxies impact parameter (D)	0.44	0.66	33.60	0.43
All galaxies luminosity (L_B/L_B^*)	2.42	0.07	92.65	1.79
All absorbers redshift (z)	1.47	0.23	76.95	1.20
Comparison of the $z < 0.4$ Isolated Sample with the Group Sample				
Metallicity ([Si/H])	1.81	0.06	93.65	1.86
Average impact parameter (D)	0.22	0.90	9.55	0.12
Most luminous galaxy impact parameter (D)	0.17	0.96	4.50	0.06
Nearest galaxy impact parameter (D)	2.42	0.08	92.00	1.75
All galaxies impact parameter (D)	0.25	0.86	14.05	0.18
All galaxies luminosity (L_B/L_B^*)	1.75	0.16	84.00	1.41
All absorbers redshift (z)	0.37	0.73	26.70	0.34

redshift distribution of group environments covers a smaller range than that of isolated environments, an Anderson–Darling test cannot rule out the null hypothesis that both are drawn from the same population (1.2σ).

The galaxy redshift and luminosity relationship for the group and isolated environments is then compared in Figure 1(d). The group and isolated environment samples cover a similar range of luminosities, although the group environments only cover a range of redshifts up to $z = 0.4$.

We do not have galaxy groups or pairs above $z = 0.4$, which raises the possibility that the isolated galaxies at redshifts $z > 0.4$ may be group environments due to poorer luminosity sensitivity at higher redshifts. To test if this affects our results, we construct a subsample of the isolated galaxies with $z < 0.4$. Anderson–Darling tests between the $z < 0.4$ isolated and group environment samples find that the luminosity, total impact parameter, and redshift distributions are consistent (1.41σ, 0.18σ, and 0.34σ, respectively). Throughout the paper, we find that comparisons between group environments and both the full and $z < 0.4$ isolated environment samples are consistent, and our results are not sample-dependent.

3. Analysis

The metallicities of each group environment have been inferred using the same method describe in Pointon et al. (2019). We summarize the analysis in the following section.

3.1. Spectral Analysis

Each transition was modeled using the VPFIT software (Carswell & Webb 2014) to measure the total column density. For COS spectra, we calculated the non-Gaussian line-spread function (LSF) for each absorption profile using the details in Kriss (2011) and the corresponding lifetime position. The FUSE data were assumed to have a Gaussian LSF and a velocity resolution of 20 km s^{-1} (FWHM). For the optical data from HIRES and UVES, we assumed a Gaussian LSF and a velocity resolution of 6.6 km s^{-1}.

We searched for and identified up to 40 different ionic transitions within $\pm$400 km s^{-1} of the median redshift of the galaxy group members. We required each absorption system to have measurable H I absorption features, while additional metal lines had to have reasonably consistent kinematic structure. That is, it is expected that Mg II absorption should have similar velocity structures to Si II absorption profiles, though not necessarily to higher ionization lines, which could arise in different phases. Where velocity profiles were unsaturated and uncontaminated by other absorption features, we fit one or more Voigt components to the absorption profile. To ensure that we did not overfit the spectra, we attempted to minimize the reduced χ^2 value. However, we also required that each component still had to maintain a reasonable Doppler parameter, because extremely broad components ($b > 100$ km s^{-1} for H I and $b > 50$ km s^{-1} for metals) are not physical. In some cases, this resulted in a model that was physically motivated, rather than determined by the χ^2 value.

In some absorption profiles, blends due to either contaminating gas at other redshifts or overlapping ions were identified. In some cases, the blends were easily recognizable due to the velocity structure of the absorption profiles of other ionic transitions. However, some blends were only apparent due to the lack of consistency between the absorption profiles of different transitions of the same ionic species. Where possible, additional Voigt profile components were added to the fit to

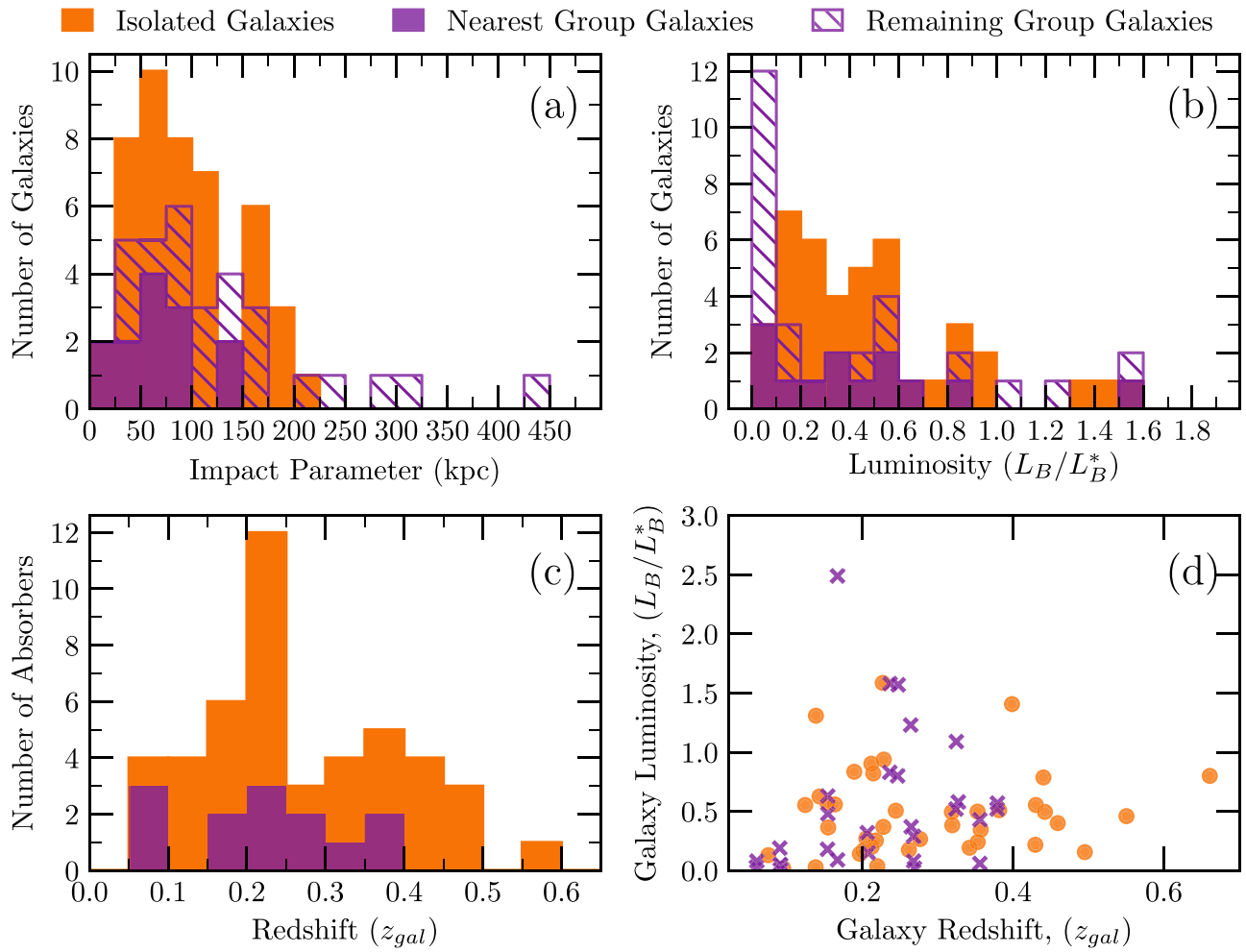

Figure 1. Distribution of isolated galaxies (orange) compared to the distribution of the nearest group galaxy members (solid purple) and all group galaxy members (hatched purple) for impact parameter (a), luminosity (b), and redshift (c). Anderson–Darling tests show that there is no significant difference between the impact parameter (0.4σ) and luminosity (1.8σ) distributions. The galaxy luminosity as a function of redshift for isolated galaxies (orange circles) and all group members (purple crosses) is shown in panel (d). Our luminosity sensitivity is comparable between the group and isolated environment samples until below $z = 0.4$, above which we currently do not have group environment data. Although the lack of group environments above $z = 0.4$ could be due to lower luminosity sensitivity at higher redshifts, our results are not dependent on selecting galaxies at all redshifts or limiting to $z < 0.4$ galaxies.

model the blend. In some cases, it was not possible to distinguish the blended absorption from the absorption profile of interest. Instead, the total column density calculated was used as a conservative upper limit on the column density. We discuss the treatment of blends for individual systems in the figure set of Figures 2.1–2.12, where we present the fits.

Many of the H I absorption profiles were saturated, making it difficult to accurately determine the H I column density. If some lines of the H I Lyman series were unsaturated or damping wings were present in the absorption profile, it was possible to obtain an accurate column density measurement. However, in the absence of unsaturated H I Lyman series transitions, there exists a degeneracy between the H I column density and Doppler parameter. That is, for a particular saturated H I column density, the Doppler parameter may vary. Therefore, increasing the number of fitted components for a saturated absorption profile will increase the H I column density. Although it is expected that the CGM is kinematically complex, resulting in many velocity components for H I, the structure cannot be determined in a saturated absorption profile. Therefore, we assume that a basic one- or two-component fit represents the lower limit on the H I column density. Due to the lack of damping wings in the absorption profile, the upper limit on the H I column density is then $\log N_{\rm H\,I} < 19.0\,{\rm cm}^{-2}$. Absorbers with column densities above this limit have damping wings that are classified as damped Lyman-alpha systems (DLAs) or sub-DLAs.[7]

Where metal transitions were saturated, we used the fit to the profile as a lower limit on the column density. If no metal absorption was detectable, we calculated 3σ upper limits on the column density using a single cloud with an assumed Doppler parameter of $b \sim 8\,{\rm km\ s}^{-1}$, derived from the average Si II Doppler parameter. Pointon et al. (2019) found no significant impact on the metallicity if a larger Doppler parameter ($b = 30\,{\rm km\ s}^{-1}$) was used.

We show the results of the fitting analysis in Figure 2 for absorption associated with the galaxy group J0228, $z_{\rm abs} = 0.2073$. The black line represents the data, the green line is the error spectrum, and the red line shows the fit to the

[7] We follow the definition in Lehner et al. (2018), Wotta et al. (2019), and Pointon et al. (2019) for the classification of H I absorbers. The H I column density ranges for pLLSs are $16.2 < \log N_{\rm H\,I} < 17.2$, LLSs have $17.2 \leqslant \log N_{\rm H\,I} < 19.0$, sub-DLAs have $19.0 \leqslant \log N_{\rm H\,I} < 20.3$, and DLAs have $\log N_{\rm H\,I} \geqslant 20.3$.

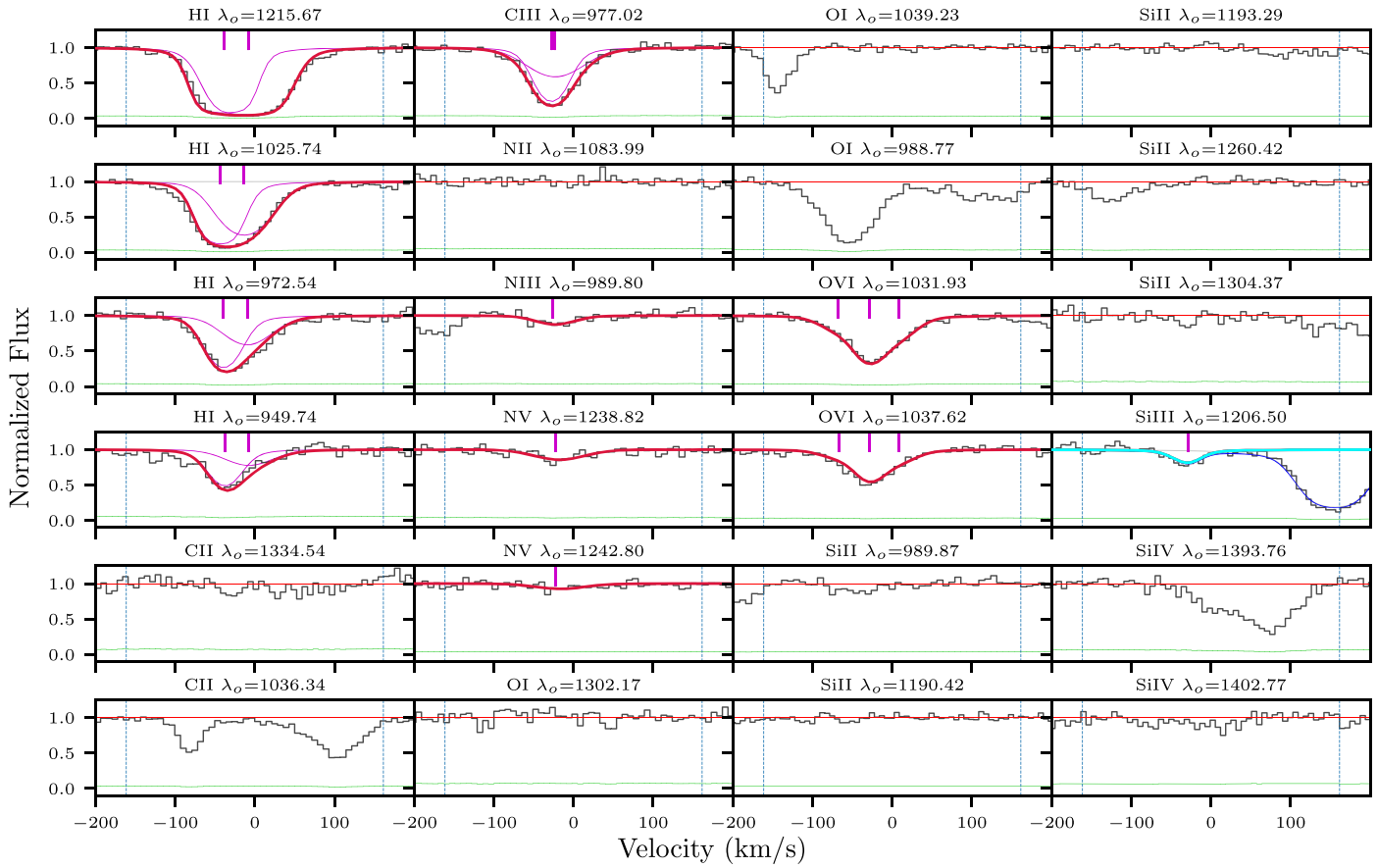

Figure 2. The fits for J0228, $z_{abs} = 0.2073$. The data for each ion (labeled above each panel) are shown in black, while the error spectrum is green. The fits to the absorption profiles are shown in red, while the components are shown in pink. The centers of each Voigt profile used to fit the absorption profile are marked with a pink tick. The zero-point of the velocity is defined by the average redshift of the group galaxy members, while the redshifts of the galaxies in velocity space are shown by blue vertical lines. For ions where we calculate limits, we show the continuum level as a thin red line. It was unclear whether the Si III transition was real or a part of the complex of lines on the positive side of the spectra. Therefore, we have assumed that the column density from the Si III fit is an upper limit, and it is shown in cyan. The total O VI fit is shown from Pointon et al. (2017) for completeness but is not used in the models. Plots for the rest of the sample are shown in the figure set of Figures 2.1–2.12.

(The complete figure set (12 images) is available.)

absorption profiles for the ionic transition labeled above the plot. The pink lines indicate the individual components used in the fit, while the pink ticks indicate the central position of each component. The redshifts of the galaxy group members are marked by vertical blue dashed lines. The velocity zero-point is defined as the average redshift of the galaxy group members. The column density measurements and limits are in Table 4 for J0228, $z_{abs} = 0.2073$. The plots of the fits and the column density data for 12 galaxy groups are shown in the figure set of Figures 2.1–2.12 and the machine readable table. We use the metallicity calculated by Muzahid et al. (2018) for J0407, $z_{abs} = 0.1670$ and do not replicate the absorption and ionization modeling.

The analysis method used enables the determination of column densities for H I Lyman series, C II, C III, C IV, N II, N III, N V, O I, Si II, Si III, Si IV, Ca II, Mg I, Mg II, and Fe II, which are then applied in the ionization modeling to determine the metallicity of the CGM. We note that the O VI column densities are presented in Pointon et al. (2017), and the fits are shown in this work for completeness.

Table 4
J0228, $z_{abs} = 0.2073$ Measured Column Densities

Ion	log N (cm^{-2})	log N Error (cm^{-2})
H I	15.26	0.02
C II	<12.79	···
C III	13.89	0.3
N II	<12.97	···
N III	13.89	0.19
N V	13.53	0.20
O I	<13.30	···
Si II	<11.78	···
Si III	<12.99	···
Si IV	<12.43	···

(This table is available in its entirety in machine-readable form.)

3.2. Ionization Modeling

A single low-ionization phase metallicity for each group environment is calculated by comparing a grid of predicted column densities modeled by the ionization modeling suite Cloudy to the column densities calculated in the previous section. Cloudy uses the input ionization conditions, set by the

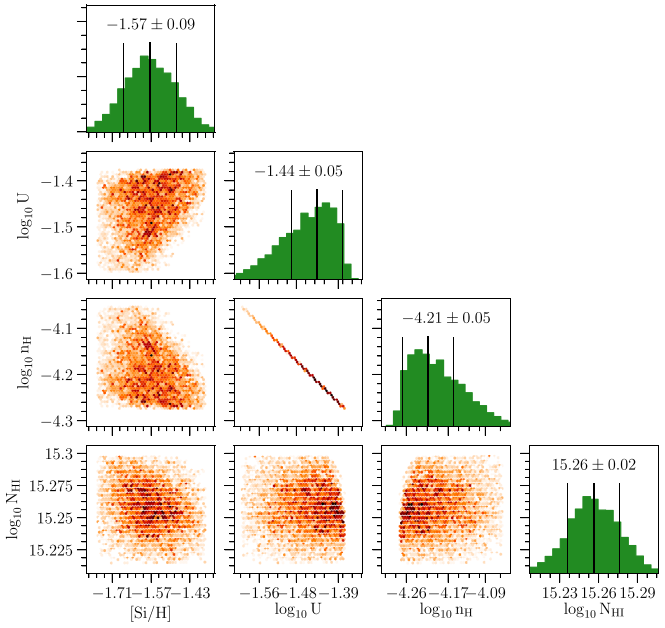

Figure 3. Posterior distribution profiles from the MCMC analysis of the Cloudy grids for J0228, $z_{\rm abs} = 0.2073$ are shown as the orange hexbin plots. The model parameters shown are [Si/H], $\log U$, $\log n_{\rm H}$, and $\log N_{\rm H\,I}$. On the end of each row, the distributions of each of those parameters are shown in green, where the 68% confidence levels and the mean are shown above and indicated by the black vertical lines. Plots for the rest of the sample are shown in the figure set of Figures 3.1–3.12.

(The complete figure set (12 images) is available.)

H I column density, $N_{\rm H\,I}$; hydrogen density, $n_{\rm H}$; and metallicity, [Si/H], to predict the column densities of the metals in the gas (Ferland et al. 2013). Typical grids cover the ranges $-5.0 < \log n_{\rm H} < -1.0\ {\rm cm}^{-3}$, $13.0 < \log N_{\rm H\,I} < 20.0\ {\rm cm}^{-2}$, and $-4.0 <$ [Si/H] < 1.5. We assumed that a uniform layer of gas with no dust and solar abundance ratios is irradiated by a background UV spectrum. The gas is also assumed to be single-phase, leading to the exclusion of the highly ionized O VI gas from the analysis. For consistency with Lehner et al. (2013), Wotta et al. (2016, 2019), and Pointon et al. (2019), we adopt the ionizing background spectrum described by the Haardt and Madau 2005 model (HM05; Haardt & Madau 2001, as implemented in Cloudy). The shape of the ionizing background, which can have an impact on the metallicity (Fechner 2011), is also assumed to only evolve with redshift.

The metallicity and ionization parameter of each absorption system are then inferred by a Markov Chain Monte Carlo (MCMC) technique described by Crighton et al. (2013). The column densities in each grid point calculated by Cloudy are compared to the measured column densities. Upper and lower limits are treated as one-sided Gaussians by the likelihood function. Priors were set to the boundaries of the Cloudy ionization grids in most cases or to the upper or lower limits of the H I column density, shown in the column density tables. For each group, we initialize the MCMC analysis with 100 walkers and a burn-in of 200 steps. The final distributions of the MCMC walkers, from which we infer the metallicity and ionization parameter, are then determined by another 200 steps.

The MCMC posterior distributions and histograms for J0228, $z_{\rm abs} = 0.2073$ are shown in Figure 3. The columns are plotted as a function of the metallicity, [Si/H]; ionization parameter, $\log U$; hydrogen number density, $\log n_{\rm H}$; and H I column density, $\log N_{\rm H\,I}$ (left to right). The posterior distributions of the MCMC walkers are shown. Darker orange indicates regions of higher probability. The final distributions of the MCMC walkers for each parameter are the green histograms at the end of each row, with the 68% uncertainties and their average or the 95% upper limit labeled above and indicated by black lines. The plots for the 12 galaxy groups analysed in this study are shown in the figure set of Figures 3.1–3.12. The ionization analysis of J0407, $z_{abs} = 0.1670$ was presented in Muzahid et al. (2018). Table 5 shows the inferred model parameters for the full sample, where we quote the most likely value, using the 68% level as the uncertainty or the 95% level for an upper limit.

4. Results

Here we present the group environment CGM metallicities and their relation to H I column densities and impact parameters. We also compare the group environment properties to the isolated galaxy properties presented in Pointon et al. (2019).

It is possible that group environments may alter the CGM metallicity. To test this, we compare the metallicity as a function of H I column density between group and isolated environments in Figure 4(a). Group absorbers are purple circles, while isolated absorbers are gray squares. Filled symbols indicate metallicity measurements, while open symbols represent limits. The group environment sample appears to overlap the isolated sample. A 1D Anderson–Darling test that accounts for upper limits indicated that the metallicity distribution of the group and isolated environment absorbers are drawn from the same population (2.4σ; 1.86σ for the $z < 0.4$ isolated sample). The median (mean) metallicity for group and isolated environments is [Si/H] $= -1.04 \pm 0.29$ (-1.07 ± 0.23) and -1.20 ± 0.16 (-1.25 ± 0.13), respectively. There is no significant difference between the median or mean metallicity for group environments compared to isolated galaxies (0.4σ or 0.5σ, respectively). Similarly, the median (mean) metallicity for the $z < 0.4$ isolated environments is [Si/H] $= -0.76 \pm 0.18$ (-0.95 ± 0.14); hence, there is no significant difference compared to the isolated sample for the median or mean (0.6σ or 0.3σ, respectively).

Using Illustris simulations, Hani et al. (2018) studied the effect of a major merger on the CGM. They found that the postmerger CGM metallicity was 0.2–0.3 dex higher than premerger. The difference in metallicity pre- and postmerger can be considered to be an upper limit on the expected metallicity difference between group and isolated environments, since the galaxies in groups may not be in the postmerger phase. However, we note that the metallicity scatter in both the isolated galaxy and group environment samples is large (>2 dex), while the sample sizes are relatively small. This limits our ability to observe a metallicity difference of 0.3 dex between the samples.

To test our ability to detect a significant difference between our samples, we attempt to predict the number of group environments that are needed to detect a 3σ difference between the mean metallicity of the group and isolated environments. We use $N = (3 \times (\sigma_g + \sigma_i)/|\mu_g - \mu_i|)^2$, where the mean and error on the mean for the group environments are represented by μ_g and σ_g, respectively. Similarly, the mean and error on the mean for the isolated environment sample are given by μ_i and σ_i, respectively. We determine that we would need to observe

Table 5
MCMC Output

J-Name	z_{abs}	Meas. $\log N_{\rm H\,I}$ [a] ($\rm cm^{-2}$)	[Si/H][b]	$\log N_{\rm H\,I}$ [b] ($\rm cm^{-2}$)	$\log n_{\rm H}$ [b] ($\rm cm^{-3}$)	$\log U$ [b]
J0125	0.3790	15.48 ± 0.02	<0.06	$15.12^{0.05}_{0.17}$	<-2.003	<-1.27
J0228	0.2073	15.26 ± 0.02	$-1.55^{-0.07}_{-0.12}$	$15.26^{0.01}_{0.02}$	$-4.246^{0.084}_{0.025}$	$-1.45^{0.03}_{0.01}$
J0228	0.2677	14.21 ± 0.01	<0.65	$14.21^{0.01}_{0.01}$	<-1.101	<-1.35
J0351	0.3251	15.26 ± 0.02	$-1.39^{-0.56}_{-0.37}$	$15.26^{0.02}_{0.02}$	$-3.779^{0.623}_{0.389}$	$-1.91^{0.32}_{0.20}$
J0407	0.0914	14.36 ± 0.01	$-0.18^{-0.06}_{-0.14}$	$14.36^{0.01}_{0.01}$	$-3.384^{0.094}_{0.094}$	$-2.43^{0.07}_{0.07}$
J0407	0.1670[c]	16.45 ± 0.05	$-0.10^{-0.02}_{-0.02}$	$16.45^{0.05}_{0.05}$	$-2.800^{0.060}_{0.060}$	$-3.20^{0.06}_{0.06}$
J0853	0.0909	14.68 ± 0.04	$-0.02^{-0.04}_{-0.10}$	$14.70^{0.04}_{0.03}$	$-3.404^{0.036}_{0.052}$	$-2.40^{0.03}_{0.04}$
J0910	0.2644	15.47 ± 0.07	$-1.04^{-0.65}_{-0.31}$	$15.45^{0.11}_{0.17}$	$-3.429^{0.971}_{-0.195}$	$-3.32^{0.94}_{-0.19}$
J0925	0.2471	19.58 ± 0.02	$-0.77^{-0.03}_{-0.02}$	$19.60^{0.02}_{0.02}$	$-3.135^{0.016}_{0.001}$	$-2.48^{0.01}_{0.01}$
J0928	0.1540	19.47 ± 0.02	$-0.23^{-0.04}_{-0.05}$	$19.47^{0.02}_{0.02}$	$-3.131^{0.045}_{0.048}$	$-2.60^{0.04}_{0.04}$
J1009	0.3556	18.96 ± 0.07	$-0.84^{-0.03}_{-0.04}$	$18.54^{0.04}_{0.03}$	$-3.081^{0.014}_{0.000}$	$-2.40^{0.01}_{0.01}$
J1119	0.0597	13.68 ± 0.02	<0.69	$13.68^{0.02}_{0.02}$	<-2.001	<-1.13
J1133	0.2366	[18.35, 19.00]	$-1.71^{-0.03}_{-0.04}$	$18.50^{0.05}_{0.08}$	$-2.919^{0.074}_{0.078}$	$-2.69^{0.07}_{0.07}$

Notes.
[a] The H I column density measured from the Voigt profile modeling of the absorption profiles.
[b] The most likely value with the 68% uncertainties from the MCMC analysis. For upper limits, we take the 95% upper uncertainty.
[c] Results from ionization modeling taken from Muzahid et al. (2018).

at least 36 group environments to observe a difference in the mean metallicity, assuming that the observed distributions are representative of the true metallicity distribution.

Previous studies have not detected an anticorrelation between the H I column density and the CGM metallicity of isolated galaxies when the HM05 ionizing background was used in the Cloudy model (Chen et al. 2017; Pointon et al. 2019; Wotta et al. 2019; Zahedy et al. 2019). The presence of an anticorrelation in Prochaska et al. (2017) is thought to be due to the use of the HM12 ionizing background (Wotta et al. 2019). We also test for the presence of an anticorrelation between the H I column density and CGM metallicity for group environments. A Kendall-tau rank correlation test, which accounts for metallicity upper limits, finds that we do not detect a significant anticorrelation between group environment CGM metallicity and H I column density (0.2σ). The details of this test and additional Kendall-tau rank correlation tests are shown in Table 6. This is consistent with the nondetection of an anticorrelation between the CGM metallicity and H I column density for isolated galaxies (2.1σ; Pointon et al. 2019). Our ability to detect an anticorrelation is dependent on the size of the sample. Due to the large scatter and limited sample size of the metallicity in group environments, it is impossible to rule out the presence of an anticorrelation.

In Figure 4(b), we present the CGM metallicity as a function of impact parameter for the group environment and isolated galaxy samples. The groups are purple, and the nearest and furthest galaxy members from the quasar sight line are represented by circles, while any other group members are marked by a purple cross, all joined by a line. The isolated galaxy–absorber pairs are gray squares. Filled symbols represent metallicity measurements, while open symbols represent metallicity upper limits. We perform Anderson–Darling tests, which account for upper limits, comparing the impact parameter distributions of the isolated sample to three different measures of impact parameter in group environments: the nearest galaxy member, the mean impact parameter, and the most luminous galaxy. We find that the differences between the isolated galaxy and the three group environment impact parameter distributions are statistically insignificant (1.7σ, 0.4σ, and 0.2σ, respectively). Similarly, the differences between the $z < 0.4$ isolated environment sample and the three group environment impact parameter distributions are statistically insignificant (1.8σ, 0.1σ, and 0.1σ) Additionally, we test for a correlation between the group CGM metallicity and the nearest galaxy impact parameter by doing a Kendall-tau rank correlation test, taking upper limits into account. We do not detect a significant relationship (1.0σ). This is consistent with Pointon et al. (2019), who found no trend between the impact parameter of isolated galaxies and the CGM metallicity, although metallicities are rarely measured beyond 120 kpc due to a lack of metal detections.

Lehner (2017) presented results investigating the metallicity of six pLLS+LLSs, where they identified more than one potential galaxy that could be associated with the absorption feature. Due to the preliminary nature of the results, the authors refrained from drawing any conclusions from the data. However, they suggested that it may be possible that for $[X/H] \geqslant -1$, the absorption systems are more likely to be associated with group environments. In contrast, absorption systems with $[X/H] < -1$ may be associated with individual galaxies in all but one absorber. We investigate this possible cause of a metallicity bimodality due to group environments by bifurcating the group and isolated samples at $[Si/H] = -1$ and comparing the relationship between the H I column density and impact parameter for high and low metallicities.

In both panels of Figure 5, the H I column density is plotted as a function of metallicity. Group environments are purple or green circles, while isolated galaxies are gray squares. Figure 5(a) shows $[Si/H] < -1$, while Figure 5(b) shows $[Si/H] \geqslant -1$. We exclude upper limits from the plot and analysis, since it is impossible to determine if they refer to high- or low-metallicity gas. While preliminary results from Lehner (2017) found that 6/7 group environments had high-metallicity CGM, we find 6/10 with high metallicity. We note that we probe a disparate H I column density range compared to Lehner (2017), who investigated pLLSs and LLSs with an H I column density range of $16.2 < \log N_{\rm H\,I} < 19.0$. However,

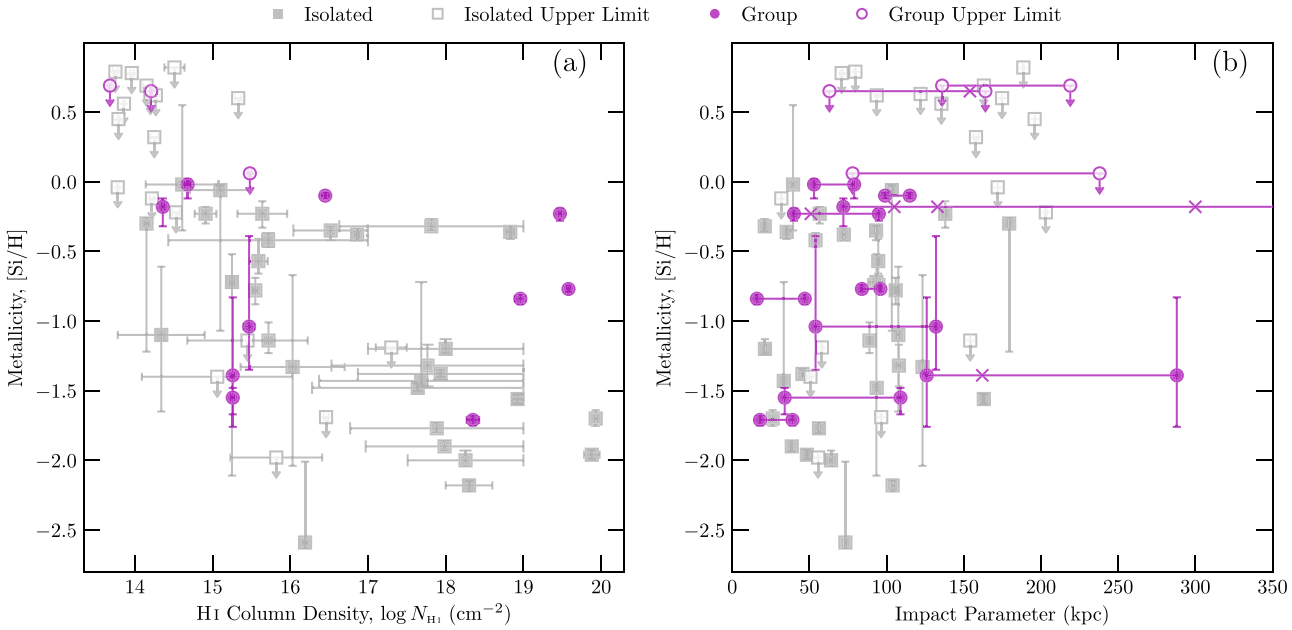

Figure 4. The CGM metallicities for group and isolated environments as a function of (a) H I column density and (b) impact parameter. Group environment CGM metallicities are purple filled circles, while metallicity upper limits are purple open circles. Isolated environment CGM metallicities are gray filled squares, while metallicity upper limits are gray open squares. Since a group has, by definition, multiple galaxies associated with a given absorption system, we plot the impact parameter of each galaxy in a group and connect these galaxies with a horizontal line. Group galaxies that are nearest to and farthest from the quasar sight line are plotted as circles, while galaxies at intermediate impact parameters are plotted as crosses.

since a comparable range of metallicities and H I column densities is observed for both group environments surveyed in this paper and isolated galaxies in Pointon et al. (2019), we suggest that the peaks of the metallicity bimodality observed by Lehner et al. (2013) and Wotta et al. (2016, 2019) are not driven by environment.

Additionally, we test for an anticorrelation between the H I column density and the impact parameter for group environments using a Kendall-tau rank correlation test for the entire sample (1.2σ), low-metallicity absorbers (1.2σ), or high-metallicity absorbers (0.2σ), where the nearest galaxy impact parameter was used. For the isolated sample, a Kendall-tau rank correlation test finds that the entire sample has a significant anticorrelation between the H I column density and the impact parameter (3.9σ). The same test on the $z < 0.4$ isolated environment sample does not find a significant anticorrelation between the H I column density and the impact parameter (2.7σ), due to the smaller sample size. Isolated galaxy high- and low-metallicity absorbers do not have significant anticorrelations between the H I column density and impact parameter (1.0σ and 1.6σ, respectively, for the full sample; 1.0σ and 1.2σ, respectively, for the $z < 0.4$ sample), likely due to the lower number of systems in each bin. Similarly, the lack of anticorrelations between the H I column density and nearest galaxy impact parameter for the entire group sample is most likely due to the limited sample size in group environments. However, if the lack of anticorrelation is due to a physical process in group environments, such as tidal stripping, higher-metallicity gas may be distributed to larger impact parameters.

It is plausible to expect that the CGM of galaxies with similar mass may be affected differently than those with higher mass ratios. Nielsen et al. (2018) found that groups with similar-mass galaxies may have larger Mg II equivalent widths and velocity dispersions compared to groups with differing-mass galaxies. Assuming that the *B*-band luminosity is a proxy for galaxy mass, we define galaxy–galaxy groups, which may later form a major merger, as those with a luminosity ratio between the most and second most luminous galaxies of $L_1/L_2 < 3.0$. In contrast, a galaxy–dwarf group, which may become a minor merger, has a luminosity ratio of $L_1/L_2 \geqslant 3.0$. To probe the effect of mass ratios on the CGM metallicity, we compare high and low metallicity for galaxy–galaxy and galaxy–dwarf groups in Figure 5. Galaxy–galaxy groups are purple circles, while galaxy–dwarfs are green circles.

We find that all but one galaxy–dwarf group has high metallicities, while galaxy–galaxy groups have both high and low metallicities. The metallicity medians (means) for the galaxy–galaxy and galaxy–dwarf group environments are -0.8 ± 0.4 (-0.7 ± 0.3) and -0.2 ± 0.3 (-0.2 ± 0.1), respectively. The median (mean) metallicities for the galaxy–galaxy and galaxy–dwarf samples differ by 1.9σ (1.1σ); thus, it is unclear if the masses of the galaxies within group environments play a role in the enrichment of the CGM.

The errors on the median or mean metallicities are highly dependent on the sample size, limiting our ability to find a significant difference in the metallicities of the galaxy–galaxy and galaxy–dwarf group environments. Therefore, we attempted to predict how many groups would be required to measure a 3σ difference between the two samples using $N = (3 \times (\sigma_{\rm gd} + \sigma_{\rm gg})/|\mu_{\rm gd} - \mu_{\rm gg}|)^2$, where the mean and error on the mean for the galaxy–galaxy sample are represented by $\mu_{\rm gg}$ and $\sigma_{\rm gg}$, respectively. Similarly, the mean and error on the mean for the galaxy–dwarf sample is given by $\mu_{\rm gd}$ and $\sigma_{\rm gd}$, respectively. We determine that we would need to observe at least six group environments in each subsample to detect a significant difference in the mean metallicity, assuming the observed distributions are representative of the true metallicity distribution.

Table 6
Kendall-tau Test Results[a]

Sample	Independent Variable	Dependent Variable	Tau Statistic	p-value	Confidence Level	σ
Rank Correlation Tests for the Isolated Sample without COS Halos Galaxies (see Section 2.5)						
Isolated	Closest galaxy impact parameter (D)	H I column density ($N_{\rm H\,I}$)	0.00	<0.01	99.52	2.82
Isolated, [Si/H] > -1.0	Closest galaxy impact parameter (D)	H I column density ($N_{\rm H\,I}$)	0.00	0.80	19.54	0.25
Isolated, [Si/H] < -1.0	Closest galaxy impact parameter (D)	H I column density ($N_{\rm H\,I}$)	0.00	0.19	81.43	1.32
Rank Correlation Tests for the Full Isolated Sample and the Group Sample						
Group	H I column density ($\log N_{\rm H\,I}$)	Metallicity ([Si/H])	−0.38	0.86	14.23	0.18
Group	Closest galaxy impact parameter (D)	Metallicity ([Si/H])	−0.38	0.33	67.48	0.98
Group	Closest galaxy impact parameter (D)	H I column density ($\log N_{\rm H\,I}$)	0.00	0.25	75.45	1.16
Group, [Si/H] $\geqslant -1.0$	Closest galaxy impact parameter (D)	H I column density ($\log N_{\rm H\,I}$)	−0.14	0.88	11.94	0.15
Group, [Si/H] < -1.0	Closest galaxy impact parameter (D)	H I column density ($\log N_{\rm H\,I}$)	0.00	0.22	77.93	1.22
Isolated	Closest galaxy impact parameter (D)	H I column density ($\log N_{\rm H\,I}$)	2.89	<0.01	99.93	3.38
Isolated, [Si/H] $\geqslant -1.0$	Closest galaxy impact parameter (D)	H I column density ($\log N_{\rm H\,I}$)	0.00	0.34	66.30	0.96
Isolated, [Si/H] < -1.0	Closest galaxy impact parameter (D)	H I column density ($\log N_{\rm H\,I}$)	0.00	0.12	88.25	1.57
Rank Correlation Tests for the Isolated Sample $z < 0.4$						
Isolated	Closest galaxy impact parameter (D)	H I column density ($N_{\rm H\,I}$)	0.00	<0.01	99.23	2.67
Isolated, [Si/H] > -1.0	Closest galaxy impact parameter (D)	H I column density ($N_{\rm H\,I}$)	0.00	0.34	66.30	0.96
Isolated, [Si/H] < -1.0	Closest galaxy impact parameter (D)	H I column density ($N_{\rm H\,I}$)	0.00	0.24	75.51	1.16

Note.
[a] We use the Kendall-tau formulation described by Brown et al. (1973), which accounts for upper limits, as implemented in ASURV (Feigelson & Nelson 1985; Isobe et al. 1986; Isobe & Feigelson 1990).

5. Discussion

Our "Multiphase Galaxy Halos" Survey has probed the CGM metallicity in 13 $z < 0.4$ group environments over a range of H I column densities ($13.6 < \log N_{\rm H\,I} < 19.6$). Typical group environments have two members, although we detect up to five in J0407, $z = 0.0914$. We do not detect a relationship between H I column density and metallicity in group environments (0.2σ), consistent with isolated environments (2.1σ; Pointon et al. 2019). However, we note that the small sample size of the groups makes it difficult to investigate this further. The lack of anticorrelation is consistent with Wotta et al. (2019), who found that LLSs and pLLSs have a metallicity range of $-3 < [{\rm X/H}] < 0$, which narrows to $-1.8 < [{\rm X/H}] < 0$ for sub-DLAs and DLAs.

We do not detect an anticorrelation between the CGM metallicity and the impact parameter of the nearest group galaxy member. This is consistent with isolated environments where the presence of an anticorrelation could not be confirmed (Pointon et al. 2019), although simulations suggest that an anticorrelation should be present (Crain et al. 2013), since it is expected that gas metallicities should decrease to that of the IGM at larger impact parameters. Small number statistics and large scatter in the CGM metallicity of group environments may explain the nondetection of an anticorrelation with impact parameter. However, it may also be possible that the IGM at the low redshifts probed by Pointon et al. (2019) and this study is sufficiently polluted by outflows that the difference between the IGM and CGM metallicities has become difficult to detect with current sample sizes. Group environments further complicate the picture. Nielsen et al. (2018) found that group environments can distribute cool Mg II gas through an intragroup medium. If it is assumed that Mg II detections are analogous to CGM metallicity detections, we can predict that an intragroup medium would also result in a flatter relationship between CGM metallicity and impact parameter. Unfortunately, it is not possible to determine if the lack of relationship between CGM metallicity and impact parameter in group environments results from an intragroup medium due to the small sample size.

It has been found in simulations that the postmerger CGM metallicity is 0.2–0.3 dex higher than premerger (Hani et al. 2018). While the difference between the mean CGM metallicities of group and isolated environments is on the order of 0.2 dex, we do not detect a significant difference between the metallicity distributions. This indicates that the CGM metallicity of group environments does not differ from that of isolated environments, although we predict that increasing the sample size of group environments to 36 may result in a significant difference. However, it is important to note that the group environments in this survey are loose groups and may not yet be gravitationally bound. The lack of difference between the CGM metallicity of group and isolated environments is consistent with the possibility that any interactions in the group environments have not yet had sufficient time to increase the metallicity and that differences between group and isolated environment metallicities may only be detected for major mergers similar to the event simulated by Hani et al. (2018).

Using the FIRE simulations, Anglés-Alcázar et al. (2017) found that the dominant accretion mechanism for CGM gas at $z < 1$ was through intergalactic transfer, which Pointon et al. (2019) suggested could drive the large scatter found in the metallicity distribution of isolated environments. The presence of well-mixed CGM halos in isolated environments at $z < 1$ is consistent with the view that CGM gas has already been enriched by mergers. Hani et al. (2018) found that the time required for the CGM metallicity to return to premerger values was at least 1 Gyr. Based on the difference between the minimum and maximum galaxy redshifts and standard

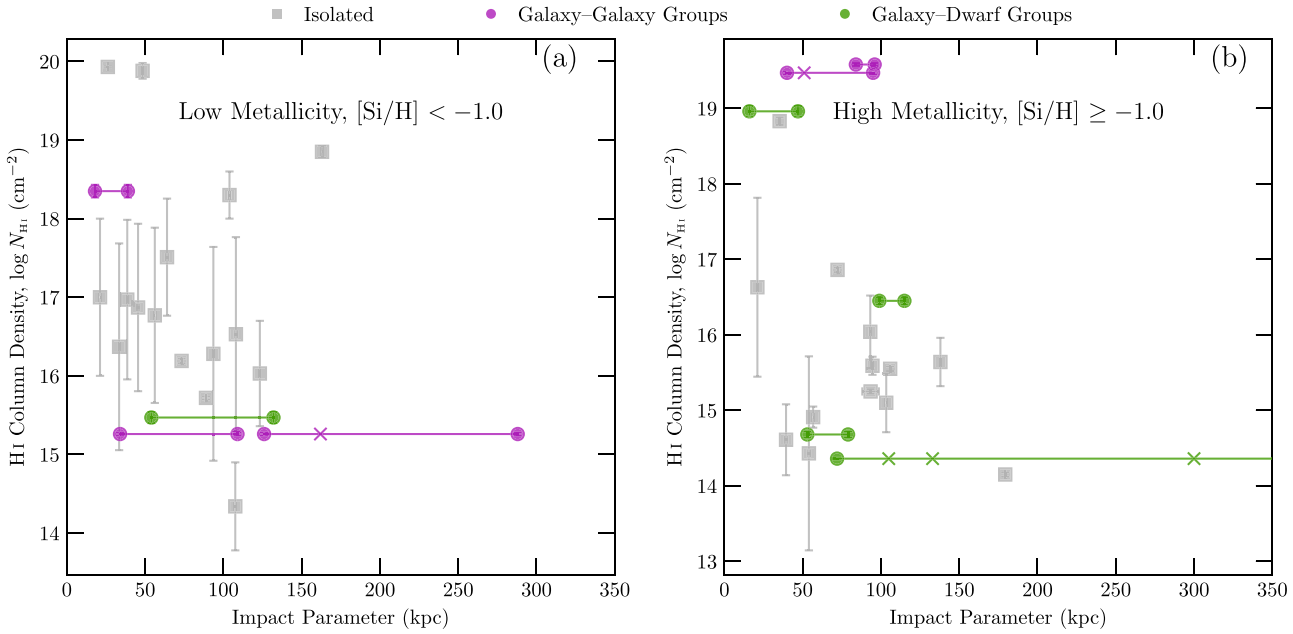

Figure 5. The H I column densities of group and isolated environments as a function of impact parameter for (a) low metallicity ([Si/H] < -1.0) and (b) high metallicity ([Si/H] $\geqslant -1.0$). Galaxy–galaxy and galaxy–dwarf group environments are in purple and green, respectively. For a given group environment, galaxies nearest to and farthest from the quasar sight line are plotted as circles, while the rest of the group member galaxies are plotted as crosses. A horizontal line is plotted for each group environment to indicate group membership. Isolated galaxies are plotted as gray squares. Limits for both the isolated and group sample have been removed, since it is impossible to determine if they correspond to high- or low-metallicity gas.

cosmology, the group environment sample covers a time span of 3.6 Gyr, while the isolated sample encompasses 5.3 Gyr (Wright 2006). Thus, it is reasonable to expect that the CGM metallicities of galaxies that experienced merger interactions over 1 Gyr earlier may have reverted to their premerger values. Alternatively, since we cannot rule out past merger events for any isolated or group galaxy, it may be possible for the CGM in both environments to have been enriched such that there is no detectable difference in metallicity at low redshifts. It is likely that a combination of these two effects has resulted in the large CGM metallicity spreads found in low-redshift isolated and group environments.

Studies of the CGM have established that the H I column density around isolated galaxies decreases with increasing impact parameter (e.g., Lanzetta et al. 1995; Tripp et al. 1998; Chen et al. 2001a; Rao et al. 2011; Borthakur et al. 2015; Curran et al. 2016; Prochaska et al. 2017; Pointon et al. 2019). However, given the flattened relationship between Mg II equivalent width and impact parameter for group environments (e.g., Chen et al. 2010a; Bordoloi et al. 2011; Nielsen et al. 2018), it is reasonable to expect that the H I may be similarly affected. Indeed, the H I column density has no significant anticorrelation with the impact parameter of the nearest group galaxy. We also do not find any anticorrelation between the H I column density and nearest galaxy impact parameter for either high ([Si/H] $\geqslant -1.0$) or low ([Si/H] < -1.0) metallicities.

However, if Mg II is assumed to be a proxy for metallicity, the stronger equivalent widths in group environments found by Chen et al. (2010a), Bordoloi et al. (2011), and Nielsen et al. (2018) are somewhat in tension with our finding that the CGM metallicity distribution is not significantly different from that of isolated galaxies. However, it is important to note that of the 7/13 group environments in the survey where Mg II was covered, there were four absorbers and three nonabsorbers. The inferred metallicities for 9/13 galaxies were dependent on the high ionization states of N V, Si IV, or C IV. Therefore, the assumption that Mg II is a proxy for metallicity does not hold for all group environments. Studies of the highly ionized gas in group environments have found that oxygen and carbon tend to be ionized above O VI and C IV (e.g., Burchett et al. 2016; Oppenheimer et al. 2016; Pointon et al. 2017; Ng et al. 2019). Therefore, it is possible that combining a single-phase gas model with highly ionized gas has led to the metal content of carbon, nitrogen, or silicon being underestimated, resulting in lower metallicities.

Lehner (2017) also investigated the relationship between H I column density and impact parameter for group environments. While they did not draw any conclusions from their preliminary results, they found a hint that low-metallicity systems could be associated with isolated environments, while high-metallicity absorbers may be associated with groups. Following this suggestion, after bifurcating the metallicity of group environments at the center of the bimodal metallicity distribution found by Lehner et al. (2013) and Wotta et al. (2016, 2019; [Si/H] $= -1.0$), we find that groups are scattered across both high (6/10) and low (4/10) metallicities. This indicates that a wide range of CGM metallicities, as opposed to only high metallicities, are associated with group environments and that galaxy environments may not be the source of the metallicity bimodality.

The mass ratios of the galaxies in group environments have been found to have an effect on the Mg II absorption (Nielsen et al. 2018), where groups with similar member galaxy luminosities may have larger equivalent widths and velocity dispersions than groups with different member galaxy luminosities. The authors suggested that galaxy–galaxy group environments may be more efficient at causing enhanced star formation and/or tidal stripping of gas. We used the *B*-band luminosity ratio as a proxy for galaxy mass to classify groups as galaxy–galaxy ($L_1/L_2 < 3.0$) or galaxy–dwarf

($L_1/L_2 \geqslant 3.0$) group environments. Using the same metallicity cut ([Si/H] $= -1.0$) as Lehner (2017), we found that all but one galaxy–dwarf group environment were associated with high-metallicity gas, while galaxy–galaxy groups were associated with both high- and low-metallicity gas. Although we did not find a significant difference in the median or mean metallicities of galaxy–galaxy and galaxy–dwarf group environments, a simple model of the group subsamples predicts that observing nine or more high- and low-metallicity group environment CGM absorbers could find a significant difference between the means of the subsample metallicities. We note that many of the inferred metallicities rely on highly ionized gas phases. However, previous studies of O VI and C IV in group environments have found that the high halo mass is sufficient to push oxygen to higher ionization states (Burchett et al. 2016; Oppenheimer et al. 2016; Pointon et al. 2017; Ng et al. 2019). Galaxy–galaxy group environments may have sufficient mass to have further ionized carbon, nitrogen, or silicon, resulting in an underestimation of the metal content of the gas, which, in turn, could result in lower metallicities. However, galaxy–dwarf environments may not yet have sufficient mass, and hence temperature, to further ionize the CGM.

The metallicities in this study were calculated using the total column density along the line of sight in the absorber. However, studies of the CGM metallicity around isolated environments have found that the metallicity is not constant across an absorption profile (e.g., Churchill et al. 2012; Crighton et al. 2015; Muzahid et al. 2015; Peeples et al. 2019; Rosenwasser et al. 2018; Zahedy et al. 2019). In essence, this means that low-metallicity gas along the line of sight can be obscured by the presence of high-metallicity gas structures, such as accretion, outflows, and tidal streams. This effectively masks any information about the structure of metals in the CGM. Future studies should attempt to calculate the metallicity structure of each individual absorber, which may assist in determining the characteristics of the CGM in group environments.

Although integrated line-of-sight metallicities may obscure some low-metallicity gas, nearly half of the metallicity measurements in group environments are metal-poor. This clearly indicates that there is a mix of high- and low-metallicity gas within group environments, similar to what is found in isolated galaxies. Using integrated line-of-sight metallicity values, it is difficult to determine if the metallicity is associated with an intragroup medium or individual galaxies within the group. Given that both O VI and Mg II absorption are associated with an intragroup medium, rather than a superposition of individual halos, it is expected that other gas traces of the halo gas in group environments would have a similar structure (Pointon et al. 2017; Nielsen et al. 2018). Component-by-component metallicity studies could reveal how individual clumps of gas within the CGM halo are amalgamated into an intragroup medium.

6. Summary and Conclusions

We used the "Multiphase Galaxy Halos" Survey to calculate the CGM metallicity of 13 $z < 0.4$ group environments. The column density for each covered ion in the absorption systems was calculated using VPFIT. These column densities were compared to the predicted column densities from Cloudy ionization models using an MCMC analysis to infer a metallicity of the absorption systems. The CGM metallicity was then compared to the H I column density of the CGM gas and the impact parameters of the group members. Our findings are as follows.

1. Group environment CGM metallicities span a large range of $-2 < [\mathrm{Si/H}] < 0$ with a mean of $\langle[\mathrm{Si/H}]\rangle = -0.54 \pm 0.22$. These are consistent with isolated galaxy CGM metallicities ($-3.0 < [\mathrm{Si/H}] < 0$, $\langle[\mathrm{Si/H}]\rangle = -0.77 \pm 0.14$) at the 0.6σ level. There is no significant enrichment of the group environment CGM at $z < 0.4$. Indeed, the similar span of metallicities in group and isolated environments suggests that there is no general preferential association of group environments with high-metallicity gas.
2. We do not detect a significant anticorrelation between the CGM metallicity and the H I column density (0.2σ) in group environments. This is consistent with previous studies that used the HM05 ionizing background to infer CGM gas metallicities.
3. There is no significant anticorrelation between the metallicity and impact parameter of the nearest group galaxy, the mean impact parameter, or the most luminous galaxy (1.3σ, 0.2σ, and 0.1σ, respectively). This is consistent with the absence of a relationship between the metallicity and impact parameter in isolated environments. It may be possible that at low redshifts, previous interactions have enriched the surrounding IGM, resulting in a lack of correlation between impact parameter and CGM metallicity.
4. We do not detect a significant anticorrelation between the H I column density and the impact parameter of the nearest galaxy in group environments. This is contrary to what is detected in the entire isolated sample, where the H I column density has been measured to decrease as the distance from the galaxy increases. Although the lack of anticorrelation in group environments may be due to low number statistics, the flattened relationship is consistent with Mg II and O VI studies, which have found evidence for an intragroup medium.
5. We further examine the environments of the groups by bifurcating the sample at $L_1/L_2 = 3.0$ and find median metallicities of -0.8 ± 0.4 and -0.2 ± 0.3 for low (galaxy–galaxy) and high (galaxy–dwarf) luminosity ratios, respectively. Although there is no significant difference from the median (1.9σ), all but one galaxy–dwarf metallicity measurements have $[\mathrm{Si/H}] > -1.0$, while galaxy–galaxy group environments have both low and high metallicities. Larger samples should be able to determine if there is a difference between the CGM metallicities of galaxy–galaxy and galaxy–dwarf environments.

With our sample size, we are unable to confidently detect a significant enhancement in the CGM metallicity for group environments. While we do not find any metallicity enhancement here with environment, samples larger than 36 group environments may find a more metal-rich intragroup medium. Larger samples may also find that a large luminosity ratio, and hence mass ratio, of the galaxies involved increases the metallicity. Regardless, we expect that a strong, detectable metallicity enhancement may only occur when galaxies are in the process of interacting or merging, which is not represented in our sample. Future work should focus on creating samples of

galaxy groups that are undergoing different phases of evolution, e.g., loose groups, compact groups, interactions, and mergers, to fully understand how galaxy environment affects the evolution of the CGM metallicity. Furthermore, studies should focus on understanding how the CGM metallicity differs along the line of sight of each absorption profile so that high-metallicity gas does not obscure metal-poor material. Such studies may also be able to use the information on the contribution of each group galaxy to the CGM to test for an intragroup medium or a superposition model using metallicity as a tracer.

We would like to thank John O'Meara for providing HIRES spectra, B. Wakker for providing the FUSE spectra, Nicolas Lehner for discussions on the UV ionizing background, and Neil Crighton for the MCMC analysis software and Cloudy ionization training. Support for this research was provided by NASA through grant HST GO-13398 from the Space Telescope Science Institute, which is operated by the Association of Universities for Research in Astronomy, Inc., under NASA contract NAS5-26555. S.K.P. acknowledges support through the Australian Government Research Training Program Scholarship. G.G.K., N.M.N., and M.T.M. acknowledge the support of the Australian Research Council through the Discovery Project DP170103470. Parts of this research were supported by the Australian Research Council Centre of Excellence for All Sky Astrophysics in 3 Dimensions (ASTRO 3D) through project No. CE170100012. Some of the data presented herein were obtained at the W. M. Keck Observatory, which is operated as a scientific partnership among the California Institute of Technology, the University of California, and the National Aeronautics and Space Administration. Observations were supported by Swinburne Keck programs 2014A_W178E, 2014B_W018E, 2015_W018E, 2016A_W056E, and 2017A_W248. The Observatory was made possible by the generous financial support of the W. M. Keck Foundation. The authors wish to recognize and acknowledge the very significant cultural role and reverence that the summit of Maunakea has always had within the indigenous Hawaiian community. We are most fortunate to have the opportunity to conduct observations from this mountain. Based on observations collected at the European Organisation for Astronomical Research in the Southern Hemisphere under ESO programs listed in Table 2.

ORCID iDs

Stephanie K. Pointon https://orcid.org/0000-0002-3846-0980
Nikole M. Nielsen https://orcid.org/0000-0003-2377-8352
Michael T. Murphy https://orcid.org/0000-0002-7040-5498
Sowgat Muzahid https://orcid.org/0000-0003-3938-8762
Christopher W. Churchill https://orcid.org/0000-0002-9125-8159
Jane C. Charlton https://orcid.org/0000-0003-4877-9116

References

Andrews, H., Barrientos, L. F., López, S., et al. 2013, ApJ, 774, 40
Anglés-Alcázar, D., Faucher-Giguère, C.-A., Kereš, D., et al. 2017, MNRAS, 470, 4698
Bielby, R., Crighton, N. H. M., Fumagalli, M., et al. 2017, MNRAS, 468, 1373
Bielby, R. M., Stott, J. P., Cullen, F., et al. 2019, MNRAS, 486, 21
Bordoloi, R., Lilly, S. J., Knobel, C., et al. 2011, ApJ, 743, 10
Borthakur, S., Heckman, T., Tumlinson, J., et al. 2015, ApJ, 813, 46
Brown, B., Hollander, M., Korwar, R. & of STATISTICS., F.S.U.T.D. 1973, Nonparametric Tests of Independence for Censored Data with Application to Heart Transplant Studies, Tech. Rep., https://ntrl.ntis.gov/NTRL/dashboard/searchResults/titleDetail/AD767617.xhtml#
Burchett, J. N., Tripp, T. M., Bordoloi, R., et al. 2016, ApJ, 832, 124
Carswell, R. F., & Webb, J. K. 2014, VPFIT: Voigt Profile Fitting Program, version 11.1, Astrophysics Source Code Library, ascl:1408.015
Chen, H.-W., Boettcher, E., Johnson, S. D., et al. 2019, ApJL, 878, L33
Chen, H.-W., Helsby, J. E., Gauthier, J.-R., et al. 2010a, ApJ, 714, 1521
Chen, H.-W., Johnson, S. D., Zahedy, F. S., Rauch, M., & Mulchaey, J. S. 2017, ApJL, 842, L19
Chen, H.-W., Lanzetta, K. M., & Webb, J. K. 2001a, ApJ, 556, 158
Chen, H.-W., Lanzetta, K. M., Webb, J. K., & Barcons, X. 2001b, ApJ, 559, 654
Chen, H.-W., & Mulchaey, J. S. 2009, ApJ, 701, 1219
Chen, H.-W., & Tinker, J. L. 2008, ApJ, 687, 745
Chen, H.-W., Wild, V., Tinker, J. L., et al. 2010b, ApJL, 724, L176
Churchill, C. W., Kacprzak, G. G., Steidel, C. C., et al. 2012, ApJ, 760, 68
Chynoweth, K. M., Langston, G. I., Yun, M. S., et al. 2008, AJ, 135, 1983
Crain, R. A., McCarthy, I. G., Schaye, J., Theuns, T., & Frenk, C. S. 2013, MNRAS, 432, 3005
Crighton, N. H. M., Hennawi, J. F., & Prochaska, J. X. 2013, ApJL, 776, L18
Crighton, N. H. M., Hennawi, J. F., Simcoe, R. A., et al. 2015, MNRAS, 446, 18
Curran, S. J., Reeves, S. N., Allison, J. R., & Sadler, E. M. 2016, MNRAS, 459, 4136
Danforth, C. W., Stocke, J. T., & Shull, J. M. 2010, ApJ, 710, 613
de Blok, W. J. G., Walter, F., Ferguson, A. M. N., et al. 2018, ApJ, 865, 26
Dekker, H., D'Odorico, S., Kaufer, A., Delabre, B., & Kotzlowski, H. 2000, Proc. SPIE, 4008, 534
Fechner, C. 2011, A&A, 532, A62
Feigelson, E. D., & Nelson, P. I. 1985, ApJ, 293, 192
Ferland, G. J., Porter, R. L., van Hoof, P. A. M., et al. 2013, RMxAA, 49, 137
Fraternali, F., van Moorsel, G., Sancisi, R., & Oosterloo, T. 2002, AJ, 123, 3124
Gauthier, J.-R. 2013, MNRAS, 432, 1444
Haardt, F., & Madau, P. 2001, in Clusters of Galaxies and the High Redshift Universe Observed in X-rays, ed. D. M. Neumann & J. T. V. Tran (Paris: Rencontres de Moriond), 64
Hani, M. H., Sparre, M., Ellison, S. L., Torrey, P., & Vogelsberger, M. 2018, MNRAS, 475, 1160
Isobe, T., & Feigelson, E. D. 1990, BAAS, 22, 917
Isobe, T., Feigelson, E. D., & Nelson, P. I. 1986, ApJ, 306, 490
Johnson, S. D., Chen, H.-W., & Mulchaey, J. S. 2013, MNRAS, 434, 1765
Johnson, S. D., Chen, H.-W., & Mulchaey, J. S. 2015, MNRAS, 449, 3263
Kacprzak, G. G., Churchill, C. W., Barton, E. J., & Cooke, J. 2011, ApJ, 733, 105
Kacprzak, G. G., Churchill, C. W., Steidel, C. C., & Murphy, M. T. 2008, AJ, 135, 922
Kacprzak, G. G., Churchill, C. W., Steidel, C. C., Spitler, L. R., & Holtzman, J. A. 2012, MNRAS, 427, 3029
Kacprzak, G. G., Murphy, M. T., & Churchill, C. W. 2010, MNRAS, 406, 445
Kacprzak, G. G., Muzahid, S., Churchill, C. W., Nielsen, N. M., & Charlton, J. C. 2015, ApJ, 815, 22
Kacprzak, G. G., van de Voort, F., Glazebrook, K., et al. 2016, ApJL, 826, L11
Kacprzak, G. G., Vander Vliet, J. R., Nielsen, N. M., et al. 2019, ApJ, 870, 137
Kriss, G. A. 2011, Improved Medium Resolution Line Spread Functions for COS FUV Spectra, COS Instrument Science Report 2011-01
Lanzetta, K. M., & Bowen, D. 1990, ApJ, 357, 321
Lanzetta, K. M., Bowen, D. V., Tytler, D., & Webb, J. K. 1995, ApJ, 442, 538
Lehner, N. 2017, Gas Accretion onto Galaxies, 430, 117
Lehner, N., Howk, J. C., Tripp, T. M., et al. 2013, ApJ, 770, 138
Lehner, N., Wotta, C. B., Howk, J. C., et al. 2018, ApJ, 866, 33
Lopez, S., Barrientos, L. F., Lira, P., et al. 2008, ApJ, 679, 1144
Meiring, J. D., Tripp, T. M., Prochaska, J. X., et al. 2011, ApJ, 732, 35
Mihos, J. C., Keating, K. M., Holley-Bockelmann, K., Pisano, D. J., & Kassim, N. E. 2012, ApJ, 761, 186
Murphy, M. 2016, UVES_popler: POst PipeLine Echelle Reduction Software, v0.72, Zenodo, doi:10.5281/zenodo.44765
Murphy, M. T., Kacprzak, G. G., Savorgnan, G. A. D., & Carswell, R. F. 2019, MNRAS, 482, 3458
Muzahid, S., Fonseca, G., Roberts, A., et al. 2018, MNRAS, 476, 4965
Muzahid, S., Kacprzak, G. G., Charlton, J. C., & Churchill, C. W. 2016, ApJ, 823, 66
Muzahid, S., Kacprzak, G. G., Churchill, C. W., et al. 2015, ApJ, 811, 132

Nestor, D. B., Johnson, B. D., Wild, V., et al. 2011, MNRAS, 412, 1559
Ng, M., Nielsen, N. M., Kacprzak, G. G., et al. 2019, ApJ, 886, 66
Nielsen, N. M., Churchill, C. W., & Kacprzak, G. G. 2013a, ApJ, 776, 115
Nielsen, N. M., Churchill, C. W., Kacprzak, G. G., & Murphy, M. T. 2013b, ApJ, 776, 114
Nielsen, N. M., Kacprzak, G. G., Muzahid, S., et al. 2017, ApJ, 834, 148
Nielsen, N. M., Kacprzak, G. G., Pointon, S. K., Churchill, C. W., & Murphy, M. T. 2018, ApJ, 869, 153
Oppenheimer, B. D., Crain, R. A., Schaye, J., et al. 2016, MNRAS, 460, 2157
Padilla, N., Lacerna, I., Lopez, S., et al. 2009, MNRAS, 395, 1135
Peeples, M. S., Corlies, L., Tumlinson, J., et al. 2019, ApJ, 873, 129
Peeples, M. S., Werk, J. K., Tumlinson, J., et al. 2014, ApJ, 786, 54
Péroux, C., Rahmani, H., Quiret, S., et al. 2017, MNRAS, 464, 2053
Pointon, S. K., Kacprzak, G. G., Nielsen, N. M., et al. 2019, ApJ, 883, 78
Pointon, S. K., Nielsen, N. M., Kacprzak, G. G., et al. 2017, ApJ, 844, 23
Prochaska, J. X., Weiner, B., Chen, H.-W., Mulchaey, J., & Cooksey, K. 2011, ApJ, 740, 91
Prochaska, J. X., Werk, J. K., Worseck, G., et al. 2017, ApJ, 837, 169
Puche, D., Westpfahl, D., Brinks, E., & Roy, J.-R. 1992, AJ, 103, 1841
Rand, R. J. 2000, ApJL, 537, L13
Rao, S. M., Belfort-Mihalyi, M., Turnshek, D. A., et al. 2011, MNRAS, 416, 1215
Rosenwasser, B., Muzahid, S., Charlton, J. C., et al. 2018, MNRAS, 476, 2258
Rubin, K. H. R., Weiner, B. J., Koo, D. C., et al. 2010, ApJ, 719, 1503
Rudie, G. C., Steidel, C. C., Trainor, R. F., et al. 2012, ApJ, 750, 67
Sancisi, R., Fraternali, F., Oosterloo, T., & van der Hulst, T. 2008, A&ARv, 15, 189
Sheinis, A. I., Bolte, M., Epps, H. W., et al. 2002, PASP, 114, 851
Steidel, C. C., Dickinson, M., & Persson, S. E. 1994, ApJL, 437, L75
Stocke, J. T., Keeney, B. A., Danforth, C. W., et al. 2013, ApJ, 763, 148
Swaters, R. A., Sancisi, R., & van der Hulst, J. M. 1997, ApJ, 491, 140
Thom, C., Werk, J. K., Tumlinson, J., et al. 2011, ApJ, 736, 1
Tripp, T. M., Lu, L., & Savage, B. D. 1998, ApJ, 508, 200
Tumlinson, J., Peeples, M. S., & Werk, J. K. 2017, ARA&A, 55, 389
Tumlinson, J., Thom, C., Werk, J. K., et al. 2011, Sci, 334, 948
Tumlinson, J., Thom, C., Werk, J. K., et al. 2013, ApJ, 777, 59
Werk, J. K., Prochaska, J. X., Thom, C., et al. 2012, ApJS, 198, 3
Werk, J. K., Prochaska, J. X., Thom, C., et al. 2013, ApJS, 204, 17
Werk, J. K., Prochaska, J. X., Tumlinson, J., et al. 2014, ApJ, 792, 8
Whiting, M. T., Webster, R. L., & Francis, P. J. 2006, MNRAS, 368, 341
Wolfe, S. A., Pisano, D. J., Lockman, F. J., McGaugh, S. S., & Shaya, E. J. 2013, Natur, 497, 224
Wotta, C. B., Lehner, N., Howk, J. C., et al. 2019, ApJ, 872, 81
Wotta, C. B., Lehner, N., Howk, J. C., O'Meara, J. M., & Prochaska, J. X. 2016, ApJ, 831, 95
Wright, E. L. 2006, PASP, 118, 1711
York, D. G., Burks, G. S., & Gibney, T. B. 1986, AJ, 91, 354
Yun, M. S., Ho, P. T. P., & Lo, K. Y. 1994, Natur, 372, 530
Zahedy, F. S., Chen, H.-W., Johnson, S. D., et al. 2019, MNRAS, 484, 2257